Scientific Research Publishing

Engineering, 2025, 17(12), 706-736
https://www.scirp.org/journal/eng
ISSN Online: 1947-394X
ISSN Print: 1947-3931

Effect of Tightening Torque on a Hybrid Stainless-Steel/Glass-Epoxy Composite Bolted Joint under Tension at Room and Cryogenic Temperature

Christian Schmitt, Pawel Lipinski, Arnaud Kremeur, Julien Capelle

National Engineering School of Metz, LEM3, University of Lorraine, Metz, France
Email: christian.schmitt@univ-lorraine.fr

How to cite this paper: Schmitt, C., Lipinski, P., Kremeur, A. and Capelle, J. (2025) Effect of Tightening Torque on a Hybrid Stainless-Steel/Glass-Epoxy Composite Bolted Joint under Tension at Room and Cryogenic Temperature. *Engineering*, **17**, 706-736.
https://doi.org/10.4236/eng.2025.1712039

Received: September 19, 2025
Accepted: December 28, 2025
Published: December 31, 2025

Abstract

The aim of this work is to study the behavior of a double-lap hybrid metallic/composite bolted joint under quasi-static tension loading at room temperature (RT) and cryogenic temperature (CT). The bolted joint is composed of two metallic stainless-steel plates and a woven glass-epoxy composite material plate. The area around the fastened hole is reinforced with a hybridization constituted by a succession of metallic stainless-steel foils and composite plies. Three-dimensional finite element analyses have been performed to evaluate the stress state in the bolted joint, especially in the vicinity of the bolt hole and in the hybridization area. The finite element model has taken into consideration the mechanical properties of the involved materials, the effects of contact between the different sheets of the assembly and the pre-stress in the bolt. The influence of the inserts (sleeves) in use around the bolt is studied to define the best geometry of the bolted joint. Three configurations were studied, namely, without a sleeve and with one or two sleeves. Finite element results have shown that the most appropriate design is a bolted joint with one sleeve. For the latter configuration, quasi-static tensile tests have been performed for several clamping force levels. Experimental results showed a moderate influence of the tightening torque on the behavior of the bolted joint, while temperature has a strong effect on the tensile strength, which increases with decreasing temperature. The fracture images showed that, in most cases, the hybrid metal/composite bolted joint failure mode corresponded to the shear-out failure.

Keywords

Bolted Joint, Glass-Epoxy Composite, Hybrid Steel-Composite, Tightening Torque, Insert, Cryogenic Temperature

1. Introduction

For the past decades, fiber reinforced polymers have been widely used in engineering fields such as aeronautics, aerospace, automotive, transport, civil engineering, naval industries or sports, thanks to their high specific mechanical properties (high strength and high stiffness to weight ratio) and good fatigue resistance. The improvement and optimization of production technologies and processes also permitted the reduction of assembly costs because polymer composite components are easy to make in a single sheet.

Nevertheless, most of the time, engineering structures are made of many components, which can be composite components only or composite and metallic components connected together. At least three techniques are usually used to connect structural composite components: mechanical fastening using riveted joints [1]-[6], bolted joints [7]-[9] and adhesive bonding joints [10]-[13]. Especially in aircraft engineering, for security reasons and for improving fatigue properties, hybrid connections based on the combination of these techniques are widely employed [14]-[19].

Bolted joints provide good convenience on inspection and maintenance compared to bonded ones; they provide the advantage of being easily replaced, if necessary, during the lifetime of the structure.

The main goal of this paper is to study the behavior of a composite/metallic bolted joint. Therefore, adhesive-bonded joints and adhesive-bolted/bonded joints are not considered here.

In literature, a lot of papers treat design, damage and strength of single-lap and double-lap bolted joints, including single-bolt and multi-bolt composite/composite and composite/metallic joints, [20]-[23] for instance. Numerous parameters such as joint geometry, bolt diameter, washer diameter, clearance between the bolt and the composite plate, clamping force which induces a pre-stress in the bolt, and stacking sequence can have a great influence on the joint behavior, changing the stress state, the stiffness and the ultimate strength of the assembly [20]-[39].

The influence of a clamping force or prestress induced by a tightening torque has been studied in numerous papers, see for instance [30] [40]-[42]. Most of the time, the experimental results show that the stiffness and the bearing strength increase as the tightening torque increases. The preload improves the bolt-hole contact and retards damage in the vicinity of the fastener hole and increases the load-carrying capacity. This is due to the friction between the contact surfaces of the components of the bolt, *i.e.*, the plates constituting the joint. In this case, no sleep between the plates can occur, and the load is transferred through the bolt by friction [40].

The effect of washer size and tightening torque on a glass-epoxy bolted joint was studied by Khashaba *et al.* [43]. It was found that the strength increases with augmenting washer size at a constant tightening torque. When the diameter of the washer decreases, lateral compressive stress in the composite material under the washer occurs and leads to micro-cracks around the hole. The stiffness of a glass-

epoxy bolted joint increases with increasing tightening torque thanks to the growth of contact pressure [43]. The role of washer size was also investigated by Sajid *et al*. [29]. A single-lap, single-bolt quasi-isotropic epoxy composite was studied. It was found that the use of larger washers permits an increase in the ultimate strength of the joint. Fengrui *et al*. [33] studied a carbon-epoxy laminate single-lap bolted joint. They found that the bolt-hole clearance had a significant influence on the distribution of load, while the bolt tightening torque had a negligible effect on it. This finding is in contradiction with the majority of studies.

The effect of the washer geometry (flat, tooth lock and spring washer) on the behavior of a quasi-isotropic glass-epoxy composite single lap bolted joint was studied by Arman *et al*. [41]. It was found that the flat washer gives a higher bearing strength thanks to a larger contact area.

The main disadvantage of riveted and bolted joints comes from the highly stressed concentration zone near the fastener hole, which can reduce the stiffness and the ultimate strength due to damage in the composite material such as matrix cracking, fiber failure or plies delamination.

In order to reduce the stress concentration factors and damages around the fastener hole and, as a consequence, to improve the bearing strength of a bolted joint, a few studies report the use of metallic or polymer inserts, or local metallic reinforcement around the hole. The case of composite bolted joints reinforced by pins [44]-[48] and the case of GLARE, *i.e*., a combination of aluminum and glass reinforced composite material [49] [50] will not be studied here.

Ferret *et al*. [51] studied a metal BigHead® insert implanted in a composite material obtained by the Resin Transfer Molding process. This kind of insert can be fitted during the manufacture of the composite. It was found that the ultimate tensile strengths in tension, compression and flexion were less for large inserts than for small ones, but no comparison with a specimen without an insert was given. Carmano *et al*. [52] studied a circular aluminum insert bonded with an epoxy adhesive to the hole of a unidirectional carbon-epoxy single lap bolted joint. They found that the maximal load is increased by 24% using this metallic insert. Muc *et al*. [53] studied a local reinforcement around the hole of a composite plate using curved fibers as the reinforcement material. The authors pointed out that this technique does not permit the recovery of the strength of the composite material without a hole, due to the great stress concentration factor in the vicinity of the hole. Mara *et al*. [54] used straight insert and insert with lap in order to improve the performance of glass/polyester double lap bolted joints and found an increase in the stiffness and ultimate load of the bolted joint with clamping force. They have shown that the use of an insert delays the damage initiation. Yingdan *et al*. [55] proposed a variable-angle tow placement technique to create local reinforcement on composite plates with holes. This technology consists of placing continuous fibers that follow the pre-calculated trajectories of eigenstresses.

However, all these technologies seem not to have yet been applied in engineering production due to the cost and process complexity.

In order to reduce the stress state level around the hole, some authors used metallic foils embedded in the composite layers.

A hybrid carbon-epoxy composite/titanium alloy assembled with a titanium bolt was studied in a few publications [56]-[58]. A local reinforcement around the hole was made with alternative carbon-epoxy and titanium alloy layers. It was found a significant increase in the strength of the bolted joint compared to this without metallic layers. Kolks *et al*. [56] studied the effect of the transition zone on the load carrying capability of a hybrid carbon-epoxy composite/ steel bolted joint subjected to combined tension-bending loading. It was found that the bearing strength was influenced by the outer steel layer alone. A spacecraft payload adaptor was made with CFRP-titanium hybrid laminates and experimentally tested [59]. The authors pointed out the advantages of this technology. They found a great increase in the load capability of bolted joints, the joint efficiency and robustness. They also pointed out a high potential for steel reinforcements.

The present study is about a metallic/composite bolted joint, particularly at cryogenic temperatures. The sequel of this bibliography is dedicated to the behavior of composite materials and composite bolted joints at low temperatures. The low temperature improves (in most cases) mechanical properties as described below. Fiber Reinforced Plastics (FRP) are a common choice for many applications at CT. One can give for examples liquid hydrogen and liquid oxygen propellant tanks of launch vehicles or rockets, composite over-wrapped vessels, aircraft and spacecraft structures as satellites [60]-[62]. In the industrial and medical sectors, the liquefied cryogenic gases such as Nitrogen, natural gas, methane, etc., are stored in tanks [63]. In recent years, the transport of natural gas in its cryogenic state (GNL) by cargo has been developed [64]-[66].

Some authors make a distinction between low temperature and cryogenic temperature. According to the generally accepted definition, low temperatures (LT) range from −50˚C to −150˚C and cryogenic temperatures (CR) are below this range.

Cryogenic temperatures correspond to the boiling point of gases. The gases most commonly used in the industrial or aerospace fields in their liquid state are argon, helium, nitrogen, carbon dioxide, hydrogen and oxygen. Except for carbon dioxide, the boiling point of the above-mentioned gases is included in a range of about [−160˚C; −270˚C], see **Table 1**.

Table 1. Boiling point of the main gases used in engineering.

Gas	Carbon dioxide	Methane	Nitrogen	Helium	Hydrogen	Oxygen	Argon
Boiling point (˚C)	−57	−162	−196	−269	−253	−183	−186

A thirty-year-old review study about the thermomechanical properties of FRP [67] reported that, in most cases, the stiffness and bearing strength of organic matrix composites increase with decreasing temperature, while failure strain decreases as temperature decreases. For instance, tests on unidirectional glass-epoxy

laminate showed a strong increase in compressive strength and a moderate increase in tensile strength at cryogenic temperature.

More recent review studies [68] [69] have confirmed that, in general, the mechanical properties of polymer matrix composites improve with temperature diminution. However, the authors pointed out the current lack of standardization of the experimental mechanical tests at cryogenic temperature. Validate assessment procedure and failure criteria for fiber reinforced plastic laminate at cryogenic temperature are not currently available.

Yan *et al*. [70] studied a unidirectional carbon-epoxy laminate and found an increase in the 0˚ and 90˚ tensile strength, in-plane shear strength and compressive strength of about 0, 27.5, 54, 8% respectively. There are, however, some contradictory results in the literature, with some authors reporting a deterioration in mechanical properties with decreasing temperature. Myung *et al*. [71] measured a decrease of around 9% in the strength of a unidirectional carbon-epoxy composite material at −150˚C compared with that at room temperature [72]. W. J. Huang *et al*. [72] studied the effect of temperature on the shear behavior of CRFP composite materials using the short beam test method. It was found a notably higher shear strength of the composite at CT (−183˚C) than at RT and high temperature (80˚C), *i.e*., a significant enhancement in the shear loading capacity of the laminate at low temperature.

Although, as mentioned above, there are numerous consistent reports available on the thermomechanical behavior of FRP, there are, to our best knowledge, few results on the behavior of bolted joints at LT and CT. Some reports are commented below.

Soykok *et al*. [73] studied a glass-epoxy laminate composite single lap bolted joint at various temperatures between RT and −40˚. This range of temperatures corresponds to a severe freezing environment that air vehicles can be exposed but does not correspond to CT or LT as defined above. It was found an increase of bearing strength of the joint with decreasing temperature. Kashaba *et al*. [74] tested a carbon-epoxy bolted joint at −70˚C. They found an increase of 30% in the stiffness compared with that at RT. On the other hand, it was found about 10% loss of strength. Koord *et al*. [75] tested a hybrid bolted joint at RT and −55˚C. The hybrid composite was constituted of a succession of steel and Carbon-epoxy layers. They found a beneficial effect of hybridization on bearing strength compared to an only carbon-epoxy bolted joint. Nevertheless, the increase in bearing stress was less pronounced at LT than at RT.

The objective of this study is concerned by overland transport of liquefied gas by truck, *i.e*., semi-trailer. This feature involves maintaining the product at very low temperatures (from −160˚C for methane to −196˚C for nitrogen). In order to assume the most severe case and the most unfavorable conditions, the temperature chosen is −196˚C, which is the lowest temperature for gases commonly transported in liquid state.

To achieve this, the design of a cryogenic semi-trailer is based on the principle

of the Dewar vessel (a double-walled container). Such the design principle is used to minimize a heat exchange with the outside by addressing the three phenomena of heat transfer (conduction, convection, and radiation). Designers and manufacturers of this type of equipment are therefore in search of materials that exhibit both interesting mechanical and insulating properties.

It is well known that metallic alloys such as Titanium, Aluminium and Steel have a high thermal conductivity (λ). In the case of a 304 stainless steel, it is equal to about 15 W/m/K at RT and 9 W/m/K at CT [76]. Composite materials have lower thermal conductivity than metallic materials. At RT, thermal conductivity of a unidirectional glass-epoxy composite is in a range from 0.4 to 0.9 W/m/K, while that of a unidirectional HT carbon fibre-epoxy composite ranges from 2 to 5 W/m/K at RT and 1 to 2 W/m/K at CT, respectively [67] [77]. Consequently, a glass-epoxy composite was studied to ensure the smallest heat transfer, *i.e.*, the best thermal insulation. In addition, the cost of a glass reinforced plastic is lower than a carbon one.

The paper is organized as follows.

In Section 2, the bolted joint studied is described, *i.e.*, its geometry, the size of the sample and its components (bolt, plates and insert) and the materials are defined. The principle of hybridization with stainless-steel foils embedded in the glass-epoxy laminate is explained. Finite element calculi are performed in order to evaluate the stress state in the hybrid composite material. The main goal of the modelling is to assess the influence of using cylindrical insert (sleeve) around the bolt and identify the less stressed configuration of the assembly. The description of the experimental study, in particular, the experimental set-up built to carry out the tensile tests at CT is described. The manufacturing of the sample is explained.

In Section 3, experimental results are shown and analysed and discussed. From the load-displacement curves at RT and CT, the stiffness, the critical and ultimate loads are determined. The comparison between the results at RT and CT are developed. The fracture images of the samples are analysed to determine the failure modes.

2. Materials and Methods

2.1. Components of the Bolted Join Studied

The bolted joint is based on the principle of the double lap bolted connection and is designed as a multi-material assembly. The model shown in **Figure 1** is used and subjected to tension loads.

It is composed of:

- two 304 L stainless-steel external plates. Their length, width and thickness are respectively $l_s = 150$ mm, $w_s = 50$ mm and $t_s = 10$ mm. A metallic bead is placed between the two plates (not represented in **Figure 1**) to allow an efficient clamping of the specimen into the first grip of the testing machine in experimental tests.
- a hybrid composite material plate of the same length and width as the metallic

plates (l_c = 150mm, w_c = 50mm) and the thickness of t_c = 5 mm. It is composed of a succession of metallic and composite layers. The stacking sequence is symmetric, in order to avoid undesired warping phenomenon during the tension or compression loading. It is composed of six 0/90 balanced woven glass-epoxy plies and four 304 L stainless steel layers. Each layer has the same thickness t_l = 0.5 mm (Figure 2(1)). A gradual transition of the length of the metallic layers is used. The metallic layers near the middle plane of the joint are 5 mm longer than the metallic plates (Figure 2(2)).

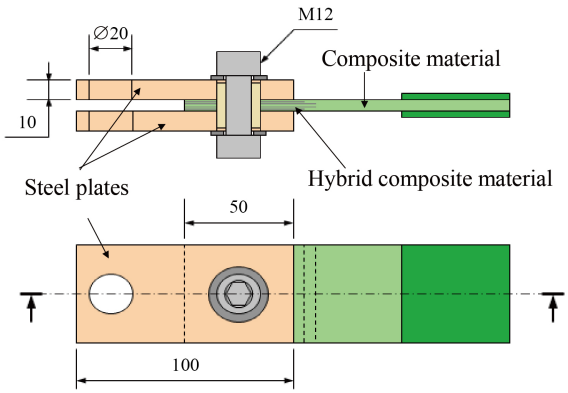

Figure 1. Design of the sample indicating all parts of the bolted joint (sizes in mm).

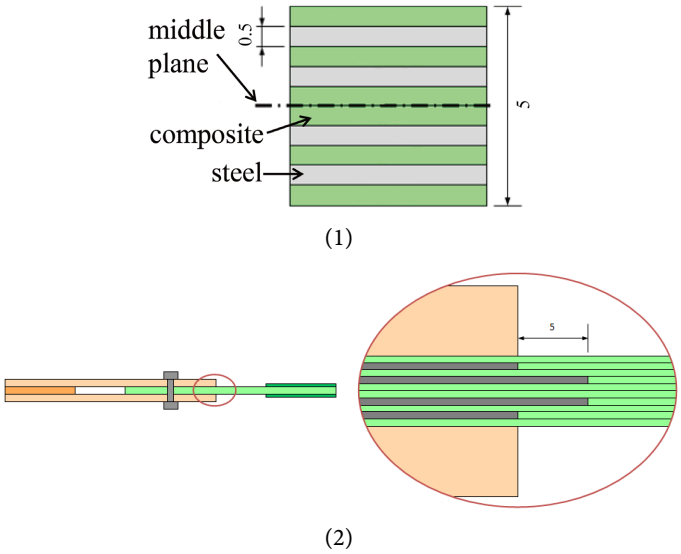

Figure 2. (1) Stacking sequence of hybrid stainless-steel/glass-epoxy composite material (2) Metallic and composite layers at the end of metallic plates (all sizes in mm).

- a stainless-steel M12 bolt of strength class A2-80 (yield strength σ_{eb} = 600 MPa and ultimate strength σ_{ub} = 800 MPa). The clearance between the composite material and the bolt is nil and this between the stainless-steel plates and the bolt is equal to 0.5 mm. The failure torque of this type of bolt is equal to 130 N·m (standard NF EN ISO 3506-1). As mentioned in introduction, the tight-

ening torque can affect the failure mode as well as the ultimate strength of the bolted joint. For this reason, in order to determine the potential influence of tightening on the behavior of the studied bolted joint, several torque levels were applied during experimental tests (see Section 4), namely 0 (finger tight), 27.5, 55 and 110 N·m.

Three hybrid composite bolted joints are studied, see Figure 3.

- a simple hybrid composite bolted joint (Figure 3(1)).
- a hybrid composite bolted joint with a cylindrical insert, or cylindrical sleeve, of an external diameter d_{1s} = 20 mm separating the bolt and the composite part. In this case, the metallic bolt remains in contact only with the metallic insert (Figure 3(2)).
- a hybrid composite bolted joint with two sleeves and a shoulder (Figure 3(3)). The first sleeve has the same external diameter (d_{1s} = 18 mm) and its length is greater than the thickness of the hybrid composite. The second sleeve has an external diameter d_{2s} = 20 mm as previously to avoid the contact between the hybrid composite and the metallic bolt.

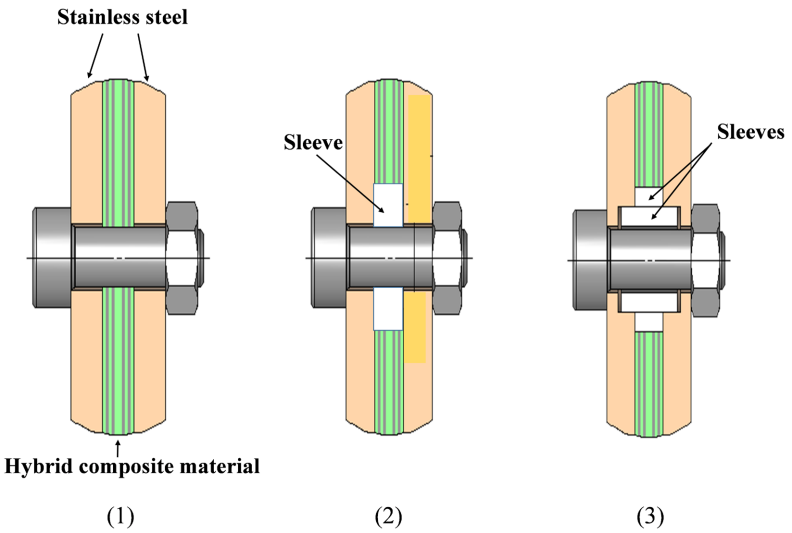

Figure 3. Three configurations and details of the hybrid composite bolted joints: (1) simple, (2) with one sleeve, (3) with two sleeves (the washer is not represented).

The main function of the bolted joint is to transfer the load from the metallic to the hybrid composite part. The three configurations were analyzed by finite element method in Sub-Section 2.2 to identify the less stressed configuration which next was tested experimentally, see Sub-Section 2.3.

2.2. Finite Element Modeling

Tension tests were modelled using the finite element method. The software MSC Marc Mentat® was used. All the components of the bolted joints are modelled considering the particular constitutive behavior of the different materials, the non-linearity due to the contact, if existing, between the different sheets of the sample

as well as the pre-stress in the bolt. Since the aim of the finite element modeling was only to define the best geometry of the bolted join, all the calculi were performed assuming a RT.

2.2.1. Meshing

A three-dimensional model is built to simulate the bolt joint under tension. The specimens have been meshed with 8 nodes hexahedral elements using HyperMesh software. Figure 4 shows a typical example of a mesh. For each configuration, ten tests were performed with various element sizes to ensure the convergence of the numerical solution. The convergence was achieved for the elements' dimensions below.

The steel plates are modelled with 5 elements through the thickness (Z-direction), each element being 2 mm thick. Concerning the composite, Z-direction element size was chosen to be equal to that of each ply, *i.e.*, 0.5 mm.

The mesh was sufficiently refined in the vicinity of the hole in the composite and steel plates in order to increase the accuracy in local area and predict the stress level correctly.

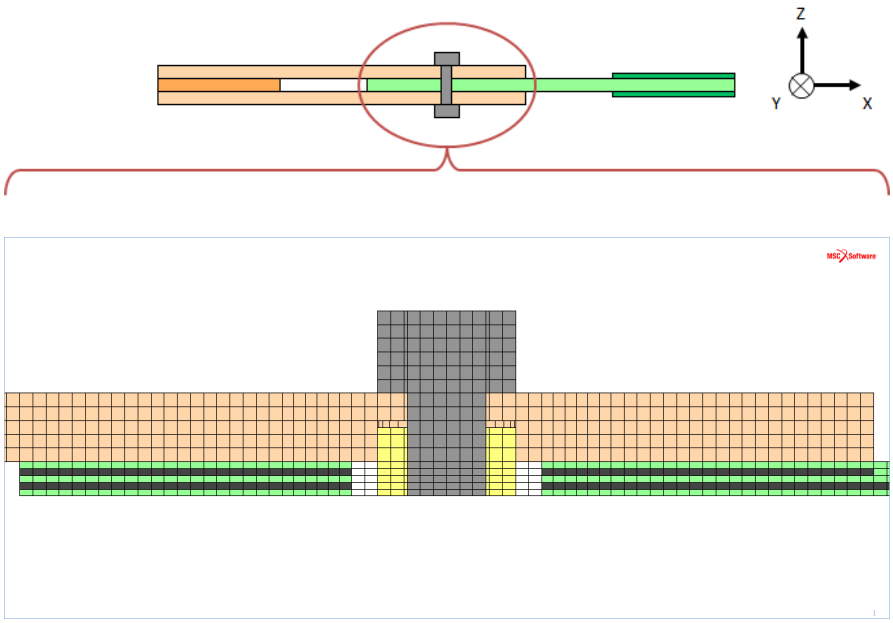

Figure 4. Example of typical mesh.

2.2.2. Mechanical Properties of the Materials Involved

The behavior of each material of the bolted joint is assumed to be homogeneous, elastic and linear.

The stainless steel is supposed isotropic with Young's modulus E_{st} = 195,000 MPa and Poisson's ratio v_{st} = 0.3.

The balanced woven composite material is supposed to be orthotropic. Its characteristics are shown in Table 2 with respect to the coordinate system indicated in Figure 4.

Table 2. Mechanical properties of woven glass-epoxy composite material.

Young modulus (MPa)	Poisson ratio	Coulomb modulus (MPa)
E_x: 26 000	ν_{xy}: 0.13	G_{xy}: 5170
E_y: 26 000	ν_{yz}: 0.34	G_{yz}: 5050
E_z: 10 750	ν_{zx}: 0.13	G_{xz}: 5050

2.2.3. Loading and Boundary Conditions

As mentioned above, the aim of the simulations by finite element method is to choose the most appropriate bolted joint among the three configurations described in previous section. The risk of damage and fracture is not considered during the analysis of obtained results. The tensile strength of the woven composite material is supposed to be equal to 500 MPa. Consequently, the applied nominal tensile stress is limited to 70% of the material strength, *i.e.*, is taken equal to $\sigma_{xx}^{\text{nom}} = 350$ MPa .

To reduce the computation time, only a quarter of the sample is modeled thanks to the symmetries of the configurations studied.

2.2.4. Modeling of Clamping Force

The pre-stress is usually taken equal to 90 percent of the yield stress of the bolt material. In the current study, the bolt class A2-80 was considered with a yield stress equal to 600 MPa and an ultimate stress equal to 800 MPa. Accordingly, the maximal admissible pre-stress in the bolt is then 540 MPa.

In order to generate the pre-stress, a thermal loading step is used. To simulate a tightening stress on the bolted joint, a negative uniaxial thermal strain is engendered in bolt using the linear thermal expansion of the material:

$$\overline{\overline{\varepsilon}}^{th} = \overline{\overline{\alpha}}\Delta T \tag{1}$$

where ΔT is the negative increment of temperature and $\overline{\overline{\alpha}}$ is a tensor of expansion coefficients such that only the component α_{33} is non nil:

$$\overline{\overline{\alpha}} = \begin{pmatrix} 0 & 0 & 0 \\ 0 & 0 & 0 \\ 0 & 0 & \alpha_{33} \end{pmatrix} \tag{2}$$

Such a tensor enables avoiding undesired thermal expansion in transverse directions of the bolt studied.

The value of ΔT is chosen to obtain the desired pre-stress in the bolt. $\Delta T = -172$ K was necessary to obtain a pre-stress equal to 540 MPa using $\alpha_{33} = 1.5 \times 10^{-5}$/K.

2.2.5. Contacts

The bolted joint is constituted of two types of materials, metallic and composite components. Some contacts are managed between the different parts and the materials.

For a steel/steel contact, a friction coefficient equal to 0.1 has been used. For a steel/glass-epoxy composite, a friction coefficient equal to 0.6 has been applied [78].

2.2.6. Stress Field Analysis

The plies of the woven composite material are supposed to be perfectly bonded one to each other. Similarly, the adjacent layers of stainless-steel and composite plies are also supposed to be perfectly bonded. It should be pointed out that perfect steel/composite bonding hypothesis overestimates the load transfer and underestimates the K_t. In fact, a not perfect bonding can lead to micro damages such as delamination, which can affect the strength of the bolted joint.

Due to the misorientation of the plies constituting the woven glass-epoxy composite material or the difference in elastic properties of the glass-epoxy composite and the stainless-steel, some stress tensor components are not necessarily continuous through the interface between two consecutive layers.

In finite element method, stress components are calculated at the Gauss points of each element. The number and location of these points depend on the element type used. For hexahedral 8 node-elements employed here, in the case of full integration technology, the stress and strain tensors are evaluated in 8 Gauss' points. To correctly evaluate the stress state in each layer, regarding the possible discontinuities, the stress state of the given integration point was translated to the nearest node of each element. In the case of nodes belonging to the discontinuity interfaces, the "no averaging" option of the multiple values was used.

2.3. Experimental Method

2.3.1. Machining of Samples

The samples made of hybrid composite material are obtained following the procedure below. The composite plates of 1156 mm length and 1000 mm in width were produced by vacuum-assisted resin infusion technique. The materials used are:

- Glass ROVING 600T (600 g/mm^2) provided by CHOMARAT
- Epoxy resin: Araldite LY 564 – Aradur 22962
- 304L stainless-steel foils

4 mm diameter holes were drilled in the metal foils to improve resin impregnation of all plies through the composite thickness during the resin infusion technique. Samples with a length of l_c = 150 mm and a width of w_s = 50 mm were then cut from the plate using computer numerical control abrasive waterjet machine. Several tests showed that cutting by milling caused significant delamination between the metal and the composite layers, rendering the method inoperative. **Figure 5** shows the drilled holes in the metallic foils and the delamination area due to milling cutting.

2.3.2. Experimental Setup

Quasi-static tensile tests were carried out at (RT) and at (CT) on a servo-hydraulic Instron tensile machine with a load cell capacity of 100 kN. The load was applied with a displacement control mode at a constant displacement rate of 1 mm/min.

Tests at RT did not require any special equipment. Only a specimen attachment system for securing the sample to the grips of the testing machine is designed.

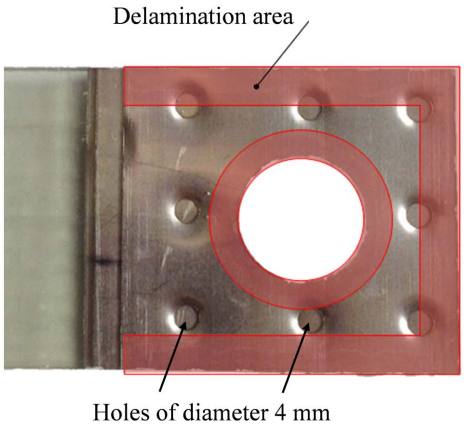

Figure 5. Detail of drilled holes in the metallic foils and the delamination area due to mechanical milling.

However, a specific device was designed for conducting tests at −196˚C corresponding to the boiling point of liquid nitrogen.

A stainless-steel tank was adapted and fixed to the lower, stationary part of the testing machine (**Figure 6**). The tank was manually filled using a cryogenic container of a liquid nitrogen reservoir equipped with a siphon tube. The tank was refilled multiple times during the test to adjust the nitrogen level due to its evaporation resulting from the heat transfer.

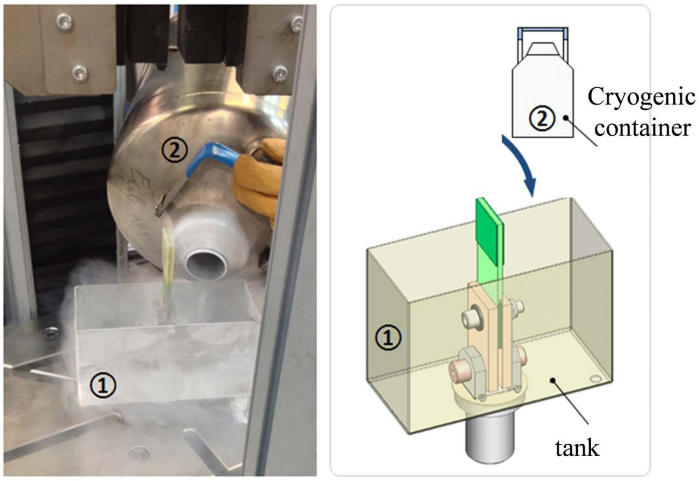

Figure 6. Tank filled with liquid nitrogen.

In order to reduce thermal exchanges with the outside, and thus limit the loss of liquid nitrogen by evaporation, the tank was insulated with 50 mm thick polystyrene panels (**Figure 7**).

Throughout the test, the bolted joint was fully immersed in the liquid nitrogen bath. Due to the low thermal conductivity of the glass-epoxy composite material, a soak time of only twenty minutes was necessary to obtain a uniform temperature in the specimen.

Figure 7. Nitrogen tank insulated with 50 mm thick polystyrene panels.

3. Results and Discussion

3.1. Choice of the Joint Configuration

The exhaustive analysis of stress distribution in the various geometric configurations of the bolted joints was done in Schmitt *et al*. [79]. The essential results concerning the three configurations studied in this paper are recalled below.

It is obvious that stresses concentrate in the vicinity of the hole when the bolted joint is mechanically loaded. But, stresses can also concentrate in the area of the interface of the composite material and the stainless steel due to the change of material stiffness (see Sub-Section 2.2.6).

To compare the behavior of the different bolted joint configurations presented in Section 2, the simplest way is to evaluate the local stress using the concept of stress concentration factor [80] defined below.

$$K_t = \frac{\sigma_{xx}^{\max}}{\sigma_{xx}^{\text{nom}}} \tag{3}$$

where σ_{xx}^{nom} is the nominal stress equal to 350 MPa in our case (see **Figure 4** for the definition of the coordinate system used). This stress level corresponds to the tension force of 87.5 kN, being the product of applied stress and the composite plate cross-section area (A = 250 mm^2). The main results of modeling are recalled below and illustrated by **Figure 8**.

For the simple hybrid bolted joint (**Figure 3(1)**), the highest σ_{xx} stress is located in the vicinity of the hole, in the composite ply at the bottom of the composite plate, see **Figure 8(1)**. The stress concentration factor reaches $K_t^{(1)} = 3.6$. In this configuration, the load is directly transmitted by the bolt to the hole since there is no clearance between the bolt and the composite plate. Mínguez *et al*. [80] found a similar result for an aluminum bolted joint, *i.e*., an increased stress concentration factor when the load is transmitted by the bolt compared to a load transmitted by the plates. In the case of simple joint, the steel foils embedded in the composite material do not permit to improve significantly the load capacity of the hybrid bolted joint.

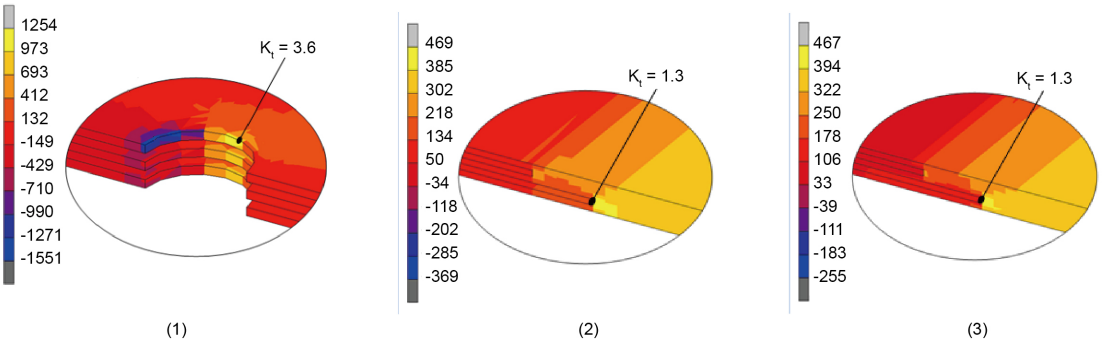

Figure 8. Color map of σ_{xx} stress component (MPa).

For hybrid bolted joint with one sleeve (**Figure 3(2)**), maximal stress does not occur in the vicinity of the hole because of no contact between the composite part and the bolt. It is localized at the end of the longest metallic ply. The stress concentration factor in tension reaches $K_t^{(2)} = 1.3$, see **Figure 8(2)**.

For hybrid bolted joint with two sleeves (**Figure 3(3)**), maximal stress in tension occurred at the end of the longest metallic ply, in the same way as for a hybrid bolted joint with a sleeve. The stress concentration factor in tension reaches comparable value of $K_t^{(3)} = 1.3$, see **Figure 8(3)**.

Consequently, the configuration (2) with one insert was chosen for experimental tests because of the additional manufacturing costs involved in fitting the second insert due to the machining of the shoulder.

3.2. Force-Displacement Curves

The typical force-displacement curve of bolted joint is drafted in **Figure 9**. Four different stages can be easily recognized. The stage I corresponds to the beginning of the loading process, at very small load in a range of about 5% of maximal force. During this stage, the relationship between force and displacement is quasi-linear. Here, no slip is acting, and the load is transferred through the friction force at the contact surface between the outer steel plates and the inner composite plate. The joint stiffness is determined by the stiffness of the composite which leads to a low slope of the curve.

During a transition stage II, the bolted joint behaves nonlinearly. Once the applied load exceeds the static friction force, the steel and the composite plates begin to slide respectively. The relative slip between the plates continues until the bolt component contacts sleeve component around it. The end of this stage corresponds to the full intimate contact between these components.

When full contact pointed out above is achieved, the applied load is mainly transferred by the interaction of the bolt against the sleeve and bolt hole. The linear portion of the force-displacement curve corresponds to stage III. The sleeve and the bolt are subjected to a shear force and a bending moment. Nevertheless, no significant deformation of the bolt and the sleeve is observed during the tensile tests. The end of stage III corresponds to critical force F^e that defines the limit of the elastic domain of the joint.

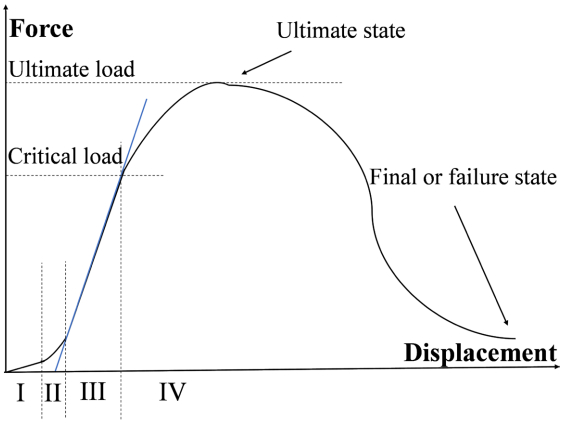

Figure 9. Four stages of a load-displacement curve. Definition of ultimate and critical loads.

The stage IV begins when the bolted joint commences to behave no-linearly, corresponding first to its elastic-plastic behavior. The force and displacement increase until the maximal value of the load, *i.e.*, until the ultimate force F^u, after which the bolted joint loses its carrying capability, *i.e.*, the load decreases as the displacement increases until complete failure of the joint. The failure force F^f is not defined from the 5% offset method because this one is usually rather used for the experimental determination of yield strength.

The failure force F^f is defined here as the force for which the bolted joint has lost 90% of its ultimate strength. So, as a result:

$$F^f = 0.1F^u$$

This choice is motivated by the fact that at the end of the experimental force-displacement curves, the displacement increases significantly while the load decreases very little.

Tensile tests were performed at RT and at CT, *i.e.*, −196˚C. Four tightening torque levels were used, namely 0, 27.5, 55 and 110 N·m. For each configuration (temperature and torque value), two samples were tested, *i.e.*, sixteen tensile tests were performed. Figure 10 and Figure 11 show the tensile test curves at RT and CT respectively. By analyzing these curves, it becomes clear that they are characterized, in most cases, by the existence of four stages discussed above.

The general appearance of these curves is similar unless the finger tight curve (in blue) at CT. However, in cryogenic temperature, and especially after the ultimate load was reached, numerous "saw-teeth" appeared on all the curves due to a probable unstable development of internal damage during the stage IV. This phenomenon is especially visible in the case of finger tight for which an unexpected sample behavior was recorded. The stage III of this curve is very short and prolonged by a slow increase of relatively moderate force of stage IV persisting until the ultimate load. It is supposed that sample damage propagated under almost constant force of about 30 kN.

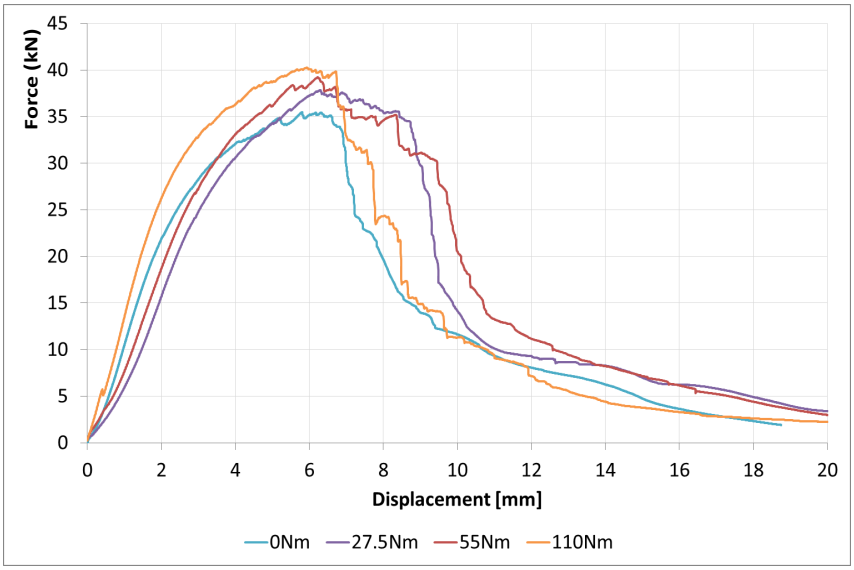

Figure 10. Force-displacement curves at RT.

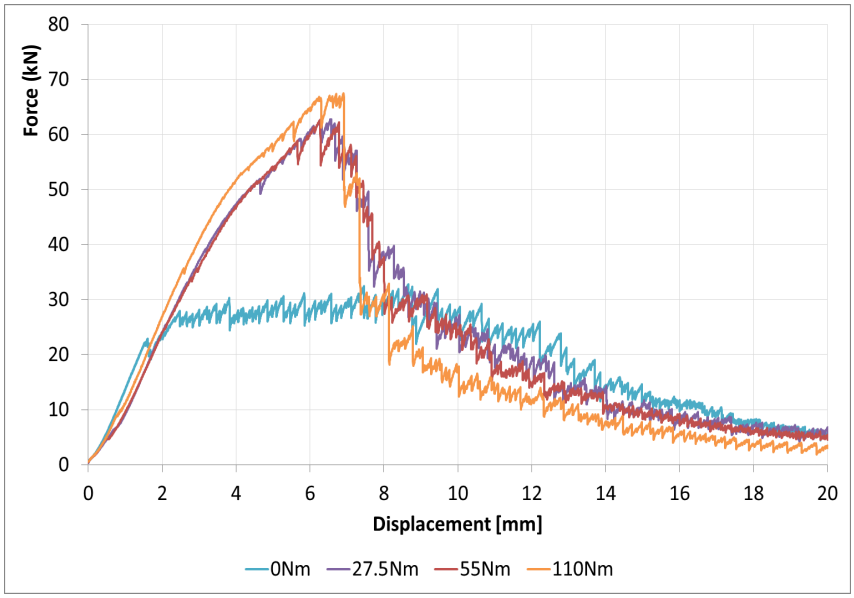

Figure 11. Load-displacement curves at CT.

3.3. Sample Stiffness Evaluation

To further understand the role of the tightening torque, a zoom in the origin of these curves was drawn in **Figure 12** for room (left image) and cryogenic (right image) temperatures. It should be noted that stages I and II are generally very short and the transition between them is not easy to distinguish. Except for finger tight (curves in blue) for which it does not exist, the extent of stage I increases with increasing tightening torque, for both RT and CT. The slope of all curves in linear stage I (when it exists) is about the same. It is represented by dashed lines (a) and (b), respectively, at RT and CT. Their values were estimated to be $k_{\mathrm{RT}}^{\mathrm{I}} = 4.7$ kN/mm and $k_{\mathrm{CT}}^{\mathrm{I}} = 7.8$ kN/mm.

One can also observe that the extent of stage II is very short, apart from for the red curves corresponding to the torque of 110 Nm, for which the stage II does not appear. For this configuration, one can see a sharp transition between the stage I and III. For the finger tight and a 55 N·m torque curves, it is not easy to distinguish the transition between stages I and II.

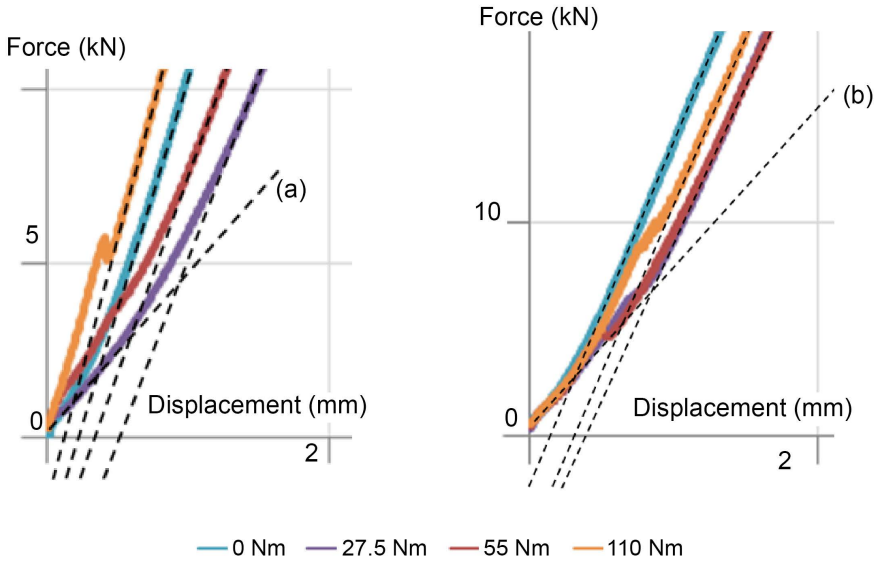

Figure 12. Zooming in the force-displacement curves at RT and CT. The dashed lines (a) and (b) correspond to the stiffness of linear stage I of the curves for a 27.5 N·m tightening torque. The other dashed lines represent the joint stiffness of linear stage III.

Table 3 gives the stage III stiffness of the bolted joint for each tightening torque. The stiffness was deduced from the slopes of the dashed straight lines in Figure 12.

Table 3. Stiffness of the bolted joint at RT and CT (−196˚C) for the different values of the tightening torque.

Tightening torque (N·m)	0	27.5	55	110	Mean
k_{RT}^{III} (kN/mm)	14	10.6	10.7	15.5	12.7
k_{CT}^{III} (kN/mm)	16.2	14.5	14.5	15.7	15.3
$\frac{k_{CT}^{III}-k_{RT}^{III}}{k_{RT}^{III}}\cdot 100$ (%)	16	37	36	1	20

At room temperature, the mean value of the stage III stiffness was about $\overline{k}_{RT}^{III}=12.7$ kN/mm . It should be noted that there is a relatively wide spread of the stiffness values at this temperature. No sound evolution of the bolted joint stiffness, as a function of the tightening torque, was found. As can be seen in Table 3, at cryogenic temperature, the tightening torque has a negligible effect on the state III stiffness of the bolted joint. Its mean value of $\overline{k}_{CT}^{III}=15.3$ kN/mm is very close

to the extremal values reported in Table 3. Also passing over the dispersion of obtained results, especially at RT, it can be remarked that the temperature has meaningful influence on the stage III stiffness of the bolted joint. In mean, the stiffness at CT is about 20% greater than its value at RT.

3.4. Critical and Ultimate Force and Displacement

As defined above, the end of stage III corresponds to critical force F^e that defines the limit of the elastic domain of the joint. The corresponding displacement is noted u^e. The values of these quantities were deduced from the experimental records illustrated in Figure 10 and Figure 11 respectively for RT and CT.

Table 4 gives the values of the critical forces for each tightening torque and both temperatures. Because the stage III is linear, the local critical stress σ_{xx}^e can be deduced from F^e using the stress concentration factor $K_t^{(2)} = 1.3$, namely: $\sigma_{xx}^e = K_t^{(2)} \frac{F^e}{A}$. The value of this stress is also given in Table 4. It can be seen that the critical load does not vary much as the tightening torque varies. Except for a finger tight, disregarding the dispersion inherent in testing, the value can be considered as constant, equal to around 22.5 kN.

Table 4 gives the values of the critical load for each tightening torque at CT. Here, in contrast to the results at RT, one observes a very clear trend, *i.e.*, an increase in critical load with tightening torque.

Table 4. Critical force and stress at RT and CT for four tightening torques.

Tightening torque (N·m)		0	27.5	55	110
RT	F_{RT}^e (kN)	18	22.7	22.6	22.4
	σ_{xx}^e (MPa)	93.6	118	118	116.5
CT	F_{CT}^e (kN)	22	30	32	34.5
	σ_{xx}^e (MPa)	114.4	156	166.4	179.4
$\frac{F_{\mathrm{CT}}^e - F_{\mathrm{RT}}^e}{F_{\mathrm{RT}}^e} \cdot 100$ (%)		22	32	42	54

At room temperature, the smallest critical force of 18 kN is obtained for a finger tight. About the same value, *i.e.*, 18 kN, is obtained when the tightening torque is not equal to zero. Applying a tightening torque induces an increase of 25% of the critical force and stress compared to a finger tight joint. The critical stress varies between 93.6 and 118 MPa. At cryogenic temperature, the influence of the tightening torque is more evident. The smallest critical force of 22 kN is obtained for a finger tight and it reaches 34.5 kN in the case of the highest tested torque. The critical stresses vary from 114.4 to 179.4 MPa respectively. In this case, the critical force and stress increase gradually with increasing torque. For tightening torque of 110 Nm the joint critical force increased about 57% compared with finger tight. The table also indicates a significant enhancement of the critical values, for each

torque, with temperature decrease. In the case of 110 N·m torque, the critical force increase is about 54% compared to the finger tight case.

Table 5 collects and compares the obtained ultimate force F^u for both testing temperatures and four tightening torques. It is recalled here that the ultimate force is defined as a maximal force reached during a test. Because the maxima are situated on the nonlinear segment of the tension curve, the stress concentration factor determined by linear analysis is no longer applicable in such a situation. The ultimate stress can't be determined by a simple role of three.

Table 5. Ultimate force at RT and CT (−196˚C) for four tightening torques.

Tightening torque (N·m)	0	27.5	55	110
F^u_{RT} at RT (kN)	35.5	37.6	38.2	40.2
F^u_{CT} at CT (kN)	31	62.9	70	67.5
$\frac{F^u_{CT}-F^u_{RT}}{F^u_{RT}}\cdot 100$ (%)	−13	67	84	68

At room temperature, as expected, the smallest bearing strength of F^u = 35.5 kN was obtained for a finger tight while the greatest one, F^u = 40.2 kN, was obtained for the greatest tightening torque. Consequently, the bearing capacity increased about 13% when comparing finger tight and 110 N·m tightening torque test results.

Similarly to RT results, the bearing strength of the bolted joints tested at CT increased with increasing tightening torque. For the reasons mentioned in the previous paragraph, the value of the bearing strengths for finger tight at CT is not considered when comparing the samples behavior at room and cryogenic temperatures.

The smallest bearing strength of F^u = 62.9 kN was obtained for a 27.5 N·m tightening torque while the greatest one of F^u = 67.5 kN was obtained for the greatest tightening torque. The application of a 110 N·m tightening torque induced an increase of 7% of bearing strength compared to the results for 27.5 N·m tightening torque. It represents rather small increase in the ultimate bolted joint performance.

In mean, the ultimate force increased about 70% when comparing the RT and CT results. However, it should be underlined that in the case of finger tight, the decrease of approximately −13% of the ultimate load was obtained at CT compared to the RT results.

The force-displacement curves of a bolted joint under tension loading have been analyzed in several studies. Most of the time, authors observed that the resulting curves can be partitioned into three or four main stages. Elastic and linear stages of load transfer occur before the internal composite damage starts. These linear stages are the most important since bolted joints are supposed to work without damage. They permit the determination of the main characteristics of the bolted joint, *i.e.*, its stiffness and its load carrying capability. Then, the progressive

damage occurs, followed by the frequently unstable bolt failure, see for instance [81]-[84].

It should be noted that the ultimate load for the different tightening torques (except finger tight) is obtained for a displacement u^e in a range of about 6 to 7 mm, both at RT and CT.

It can also be seen that the failure load is obtained for all the tests (at RT and CT) for a displacement included in a range between 18.5 and 20 mm. Once again, this failure elongation is not influenced by the testing temperature.

Consequently, the cryogenic temperature does not affect the value of ultimate and failure displacements. Similar observations have been made in [73] for a single shear lap glass-epoxy composite bolted joint tested at RT and −40˚C.

In contrast, temperature has a great influence on the ultimate and critical forces of the bolted joint. For instance, for a tightening torque of 110 Nm, the ultimate load changes from 40.2 kN at RT to 67.5 kN at CT, *i.e.*, a significant increase of 68% was obtained (**Table 4**). For the same value of the tightening torque, the critical load rose from 22.4 kN at RT to 34.5 kN at CT. It corresponds to a significant increase of 54% (**Table 3**).

3.5. Failure Mode

Damage in the vicinity of the bolt hole includes fiber breakage, matrix cracking, debonding and delamination on the fiber/matrix interface and delamination of the plies interface. The generally observed failure modes are net tension, shear-out failure, bearing, tear-out and cleavage, or a combination of two or several of these damage types, see for instance [24]-[26] [31] [74] [80] [82] [85] [86].

After the completion of each test, the bolted joint was disassembled from the test setup to examine its failure mode. Interrupted tests were also conducted. The loading of the bolted joint was stopped at the ultimate state (corresponding to the ultimate load) of the load-displacement curve. The evolution of internal damage was then examined on the composite material at two states, ultimate and final or failure state.

Figure 13 shows the fracture images for each configuration, *i.e.*, four tightening torques and two temperatures.

For almost all configurations (except finger tight at CT, see below), the photos show a fracture that looks like a tear-out failure [24] with fiber breakage. In fact, the first damage initiated at the bolted hole vicinity progresses to the small holes of diameter 4 mm in the metallic foils. So, these holes appear as an area of joint feebleness. The stress state is altered in the vicinity of the drilled foil holes. Indeed, it is well known that the presence of holes increases local stresses.

One can conclude that the failure is a shear-out failure modified by the presence of the small holes in the steel plies.

For a finger tight at CT, the failure mode corresponds to a shear-out damage in the hybrid composite material accompanied by fiber breakage in the vicinity of the hole.

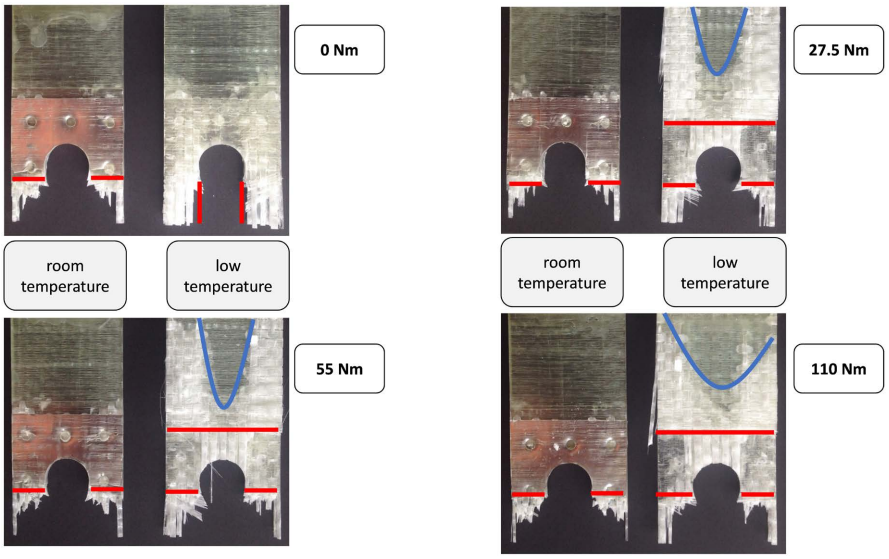

Figure 13. Fracture image of the hybrid composite material, at RT and CT, at failure state.

For a 110 N·m torque at CT, one can also identify a fiber splitting. The blue lines on the photos delimit a white area corresponding to the delamination zone into the laminate above the bolt hole. At RT, these delamination zones are not visible. At RT, the damage is concentrated around the hole, whereas at CT, the damage spreads progressively, making it possible to increase the critical and the ultimate loads. At CT, one can notice that the undamaged area decreases as the tightening torque increases which explains the beneficial effect of clamping force on the value of the ultimate load.

The metal foils are hardly distinguishable from the composite layers, which leads us to assert that the fracture occurs homogeneously in the hybrid composite. Also, it can be noted that the transition zone isn't the weakest area of the reinforcement technique. The same observation was made for a hybrid composite bolted joint composed of a carbon-epoxy with titanium foils and a titanium bolt [87].

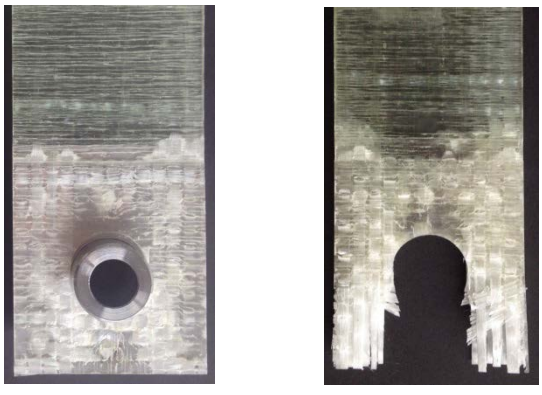

Ultimate state Failure state

Figure 14. Fracture image of the hybrid composite material for a finger tight at CT, at ultimate state and failure state.

Figure 14 shows the photos of the composite component of the bolted joint at the two states mentioned above, ultimate and final states, at CT for a finger tight. At ultimate state, one can see the complete delamination (white area) around the bolt hole. The composite is completely damaged around the bolt hole and almost all over the area reinforced with metallic foils, which explains the small values of ultimate and critical loads deduced from the load-displacement curve.

Figure 15 shows the photos of the composite laminate at ultimate and final states, for a maximal tightening torque (110 N·m) at CT. The area around the hole is not entirely delaminated. One can see the undamaged zone at the front of the bolt hole and behind it. The progression of this damage delamination leads then to failure.

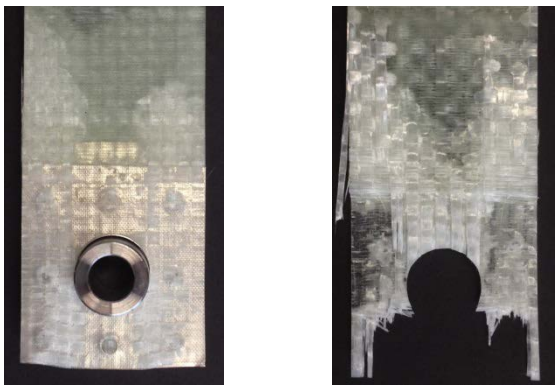

Ultimate state Failure state

Figure 15. Fracture image of the hybrid composite material for a 110 N·m tightening torque at CT, at ultimate and failure states.

4. Conclusions

Compared to hybrid metal/carbon-epoxy (titanium/carbon-epoxy and steel/carbon-epoxy) bolted joints, research on the behavior of metal/glass-epoxy bolted joints is rare. Few results of studies on composite/composite and metal/composite at cryogenic temperatures are available. This study contributes to clearing these gaps.

The paper has been devoted to studying a double-lap hybrid stainless steel/glass-epoxy bolted joint under quasi-static tension. An insert positioned around the fastened hole prevents direct contact between the bolt and the composite part of the bolted joint. Tensile tests at RT and CT were conducted to investigate the effect of clamping force and temperature on the load capacity and failure mode of the bolted joint. Based on the obtained results, the following main conclusions can be summarized as follows:

- At RT and CT, the force-displacement curves can be partitioned into four stages which correspond to load transfer respectively by the friction force, the relative slip between the metallic and composite plates, the load transfer by the bolt against the insert, and the last non-linear stage during which damage develops until the structure is ruined.

- Clamping force has a limited effect on the ultimate load value. The maximal tightening torque applied was equal to 110 N·m, corresponding to 90% of the yield stress of a class A2-80 stainless steel bolt. At RT, the bearing strength of the bolted joint increased approximately by 13% with increasing tightening torque from 0 (finger tight) to the above-mentioned maximal value. At CT, the increase was equal to 7%.

Clamping force has a negligible effect on the values of ultimate and failure displacements.

- Temperature has a great effect on the bearing strength of the bolted joint. At CT, the critical and the ultimate loads are respectively 54% and 68% higher than at RT. On the other hand, temperature has a limited effect on ultimate and failure displacements.
- The fracture images show a shear-out failure influenced by the presence of small drilled holes in the reinforcing metal sheets embedded in the composite. The stress state in the reinforcement zone is modified by the interaction between the bolt hole and the holes in the metal foils. The drilled holes appear to affect the strength of the bolted joint. It is planned to improve the specimen manufacturing process by eliminating this drill operation in the metal sheets. A practical alternative such as laser-perforated foils will be tested for future prototypes.
- It should be noted that, due to the small sample sizes, the results described in Section 3 should be confirmed by further testing.
- The use of reinforcing foil sheets embedded in the composite material, combined with an insert around the bolt to protect the composite material, is a promising approach for improving the mechanical behavior of hybrid bolted joints. It would be necessary to evaluate the fatigue strength of this type of bolted joint by performing appropriate fatigue tests.
- In the next work, the finite element model will be improved by considering the elastoplastic constitutive behavior of stainless steel and including a damage model for composite materials. This would make it possible to refine the prediction of the stress state and optimize the geometry of the bolted joint, including the arrangement and geometry of the metal foils, as well as the ratio of bolt diameter to joint width.

The use of a hybrid stainless steel/glass-epoxy composite bolted joint can lighten the mass of a cryogenic tank truck, helping to reduce fuel consumption. Above all, it reduces heat exchange and loss between the tank and the exterior at CT compared with a metal/metal bolted joint, resulting in cost savings and a beneficial effect on the environment.

Conflicts of Interest

The authors declare no conflicts of interest regarding the publication of this paper.

References

[1] Zhang, M., Cao, Z., Zheng, G., Zuo, D., Guo, C. and Wang, Y. (2024) Quasi-Static

Tensile Failure Mechanism Analysis of CFRP/Al Countersunk Electromagnetic Riveted Joints with Different Rivet-Hole Clearances. *Engineering Failure Analysis*, **155**, Article ID: 107759. https://doi.org/10.1016/j.engfailanal.2023.107759

[2] He, Z., Zheng, G., Luo, Q., Li, Q. and Sun, G. (2024) Fatigue Life Improvement Mechanisms of CFRP/Al Hybrid Joints—Load Sharing Study Using a Digital Image Correlation Technique. *Composite Structures*, **327**, Article ID: 117625. https://doi.org/10.1016/j.compstruct.2023.117625

[3] Feng, J., Zhang, J., Jin, W. and Liao, R. (2024) Damage Evolution Modeling of CFRP/Al Single-Lap Screw Type Blind Riveted Joints during Realistic Installation Process. *Composite Structures*, **337**, Article ID: 118023. https://doi.org/10.1016/j.compstruct.2024.118023

[4] Fortier, V., Brunel, J. and Lebel, L. (2019) Fastening Composite Structures Using Braided Thermoplastic Composite Rivets. *Journal of Composite Materials*, **54**, 801-812. https://doi.org/10.1177/0021998319867375

[5] Mi, S., Hu, J., Xuan, S., Yu, J. and Tian, W. (2022) An Experimental Investigation on Press Joining Mechanism and Bearing Behavior of Single-Lap Composite Riveted Joints. *Journal of Composite Materials*, **57**, 393-407. https://doi.org/10.1177/00219983221146263

[6] Lee, J., Oh, M. and Kim, H. (2023) Fatigue Strength of Self-Piercing Riveted Joints of Carbon Fiber Reinforced Composite and Al5052 Alloy Plates. *Journal of Composite Materials*, **57**, 3479-3491. https://doi.org/10.1177/00219983231167662

[7] Olivier, G., Csillag, F., Christoforidou, A., Tromp, L., Veltkamp, M. and Pavlovic, M. (2023) Feasibility of Bolted Connectors in Hybrid FRP-Steel Structures. *Construction and Building Materials*, **383**, Article ID: 131100. https://doi.org/10.1016/j.conbuildmat.2023.131100

[8] Ravichandran, B. and Balasubramanian, M. (2024) Joining Methods for Fiber Reinforced Polymer (FRP) Composites—A Critical Review. *Composites Part A*: *Applied Science and Manufacturing*, **186**, Article ID: 108394. https://doi.org/10.1016/j.compositesa.2024.108394

[9] Delzendehrooy, F., Akhavan-Safar, A., Barbosa, A.Q., Beygi, R., Cardoso, D., Carbas, R.J.C., *et al*. (2022) A Comprehensive Review on Structural Joining Techniques in the Marine Industry. *Composite Structures*, **289**, Article ID: 115490. https://doi.org/10.1016/j.compstruct.2022.115490

[10] Kupski, J. and Teixeira de Freitas, S. (2021) Design of Adhesively Bonded Lap Joints with Laminated CFRP Adherends: Review, Challenges and New Opportunities for Aerospace Structures. *Composite Structures*, **268**, Article ID: 113923. https://doi.org/10.1016/j.compstruct.2021.113923

[11] Ribeiro, T.E.A., Campilho, R.D.S.G., da Silva, L.F.M. and Goglio, L. (2016) Damage Analysis of Composite-Aluminium Adhesively-Bonded Single-Lap Joints. *Composite Structures*, **136**, 25-33. https://doi.org/10.1016/j.compstruct.2015.09.054

[12] Kang, S., Kim, M. and Kim, C. (2007) Evaluation of Cryogenic Performance of Adhesives Using Composite-Aluminum Double-Lap Joints. *Composite Structures*, **78**, 440-446. https://doi.org/10.1016/j.compstruct.2005.11.005

[13] Nguyen, K., Kweon, J. and Choi, J. (2009) Failure Load Prediction by Damage Zone Method for Single-Lap Bonded Joints of Carbon Composite and Aluminum. *Journal of Composite Materials*, **43**, 3031-3056. https://doi.org/10.1177/0021998309345295

[14] Lim, G., Bodjona, K., Raju, K.P., Fielding, S., Romanov, V. and Lessard, L. (2018) Evolution of Mechanical Properties of Flexible Epoxy Adhesives under Cyclic Loading and Its Effects on Composite Hybrid Bolted/Bonded Joint Design. *Composite*

Structures, **189**, 54-60. https://doi.org/10.1016/j.compstruct.2018.01.049

[15] Lopez-Cruz, P., Laliberté, J. and Lessard, L. (2017) Investigation of Bolted/Bonded Composite Joint Behaviour Using Design of Experiments. *Composite Structures*, **170**, 192-201. https://doi.org/10.1016/j.compstruct.2017.02.084

[16] Mohapatra, D.R., Behera, S. and Mondal, S. (2025) Modified Hashin Criteria Based 3D Damage Progression in Bolted, Bonded and Hybrid Single-Lap Joints of Woven GFRP Laminates. *Structures*, **78**, Article 109265. https://doi.org/10.1016/j.istruc.2025.109265

[17] Marannano, G. and Zuccarello, B. (2015) Numerical Experimental Analysis of Hybrid Double Lap Aluminum-CFRP Joints. *Composites Part B*: *Engineering*, **71**, 28-39. https://doi.org/10.1016/j.compositesb.2014.11.025

[18] Xiang, S., Cheng, B., Wang, J., Li, D. and Yan, X. (2024) Experimental and Numerical Investigation on Failure Behavior of Hybrid Bonded/Bolted GFRP Single-Lap Joints under Static Shear Loading. *Engineering Failure Analysis*, **158**, Article ID: 107969. https://doi.org/10.1016/j.engfailanal.2024.107969

[19] Zhang, H., Zhang, L., Liu, Z., Qi, S., Zhu, Y. and Zhu, P. (2021) Numerical Analysis of Hybrid (Bonded/Bolted) FRP Composite Joints: A Review. *Composite Structures*, **262**, Article ID: 113606. https://doi.org/10.1016/j.compstruct.2021.113606

[20] Camanho, P.P. and Lambert, M. (2006) A Design Methodology for Mechanically Fastened Joints in Laminated Composite Materials. *Composites Science and Technology*, **66**, 3004-3020. https://doi.org/10.1016/j.compscitech.2006.02.017

[21] Mandal, B. and Chakrabarti, A. (2018) Numerical Failure Assessment of Multi-Bolt FRP Composite Joints with Varying Sizes and Preloads of Bolts. *Composite Structures*, **187**, 169-178. https://doi.org/10.1016/j.compstruct.2017.12.048

[22] Nerilli, F. and Vairo, G. (2017) Progressive Damage in Composite Bolted Joints via a Computational Micromechanical Approach. *Composites Part B*: *Engineering*, **111**, 357-371. https://doi.org/10.1016/j.compositesb.2016.11.056

[23] Hu, X.F., Haris, A., Ridha, M., Tan, V.B.C. and Tay, T.E. (2018) Progressive Failure of Bolted Single-Lap Joints of Woven Fibre-Reinforced Composites. *Composite Structures*, **189**, 443-454. https://doi.org/10.1016/j.compstruct.2018.01.104

[24] Thoppul, S.D., Finegan, J. and Gibson, R.F. (2009) Mechanics of Mechanically Fastened Joints in Polymer-Matrix Composite Structures—A Review. *Composites Science and Technology*, **69**, 301-329. https://doi.org/10.1016/j.compscitech.2008.09.037

[25] Shan, M., Zhao, L., Liu, F., Qi, D. and Zhang, J. (2020) Revealing the Competitive Fatigue Failure Behaviour of CFRP-Aluminum Two-Bolt, Double-Lap Joints. *Composite Structures*, **244**, Article ID: 112166. https://doi.org/10.1016/j.compstruct.2020.112166

[26] Hizam, R.M., Manalo, A.C., Karunasena, W. and Bai, Y. (2018) Effect of Bolt Threads on the Double Lap Joint Strength of Pultruded Fibre Reinforced Polymer Composite Materials. *Construction and Building Materials*, **181**, 185-198. https://doi.org/10.1016/j.conbuildmat.2018.06.061

[27] Li, H., Gu, R. and Zhao, X. (2017) Global Sensitivity Analysis of Load Distribution and Displacement in Multi-Bolt Composite Joints. *Composites Part B*: *Engineering*, **116**, 200-210. https://doi.org/10.1016/j.compositesb.2017.01.058

[28] Liu, F., Zhang, J., Zhao, L., Xin, A. and Zhou, L. (2015) An Analytical Joint Stiffness Model for Load Transfer Analysis in Highly Torqued Multi-Bolt Composite Joints with Clearances. *Composite Structures*, **131**, 625-636. https://doi.org/10.1016/j.compstruct.2015.06.003

[29] Sajid, Z., Karuppanan, S., Sallih, N., Kee, K.E. and Shah, S.Z.H. (2021) Role of Washer Size in Mitigating Adverse Effects of Bolt-Hole Clearance in a Single-Lap, Single-Bolt Basalt Composite Joint. *Composite Structures*, **266**, Article ID: 113802. https://doi.org/10.1016/j.compstruct.2021.113802

[30] Liu, L., Zhang, J., Chen, K. and Wang, H. (2014) Combined and Interactive Effects of Interference Fit and Preloads on Composite Joints. *Chinese Journal of Aeronautics*, **27**, 716-729. https://doi.org/10.1016/j.cja.2014.04.014

[31] Russo, S. (2016) First Investigation on Mixed Cracks and Failure Modes in Multi-Bolted FRP Plates. *Composite Structures*, **154**, 17-30. https://doi.org/10.1016/j.compstruct.2016.07.016

[32] Kapidžić, Z., Ansell, H., Schön, J. and Simonsson, K. (2015) Fatigue Bearing Failure of CFRP Composite in Biaxially Loaded Bolted Joints at Elevated Temperature. *Composite Structures*, **127**, 298-307. https://doi.org/10.1016/j.compstruct.2015.03.031

[33] Liu, F., Lu, X., Zhao, L., Zhang, J., Hu, N. and Xu, J. (2018) An Interpretation of the Load Distributions in Highly Torqued Single-Lap Composite Bolted Joints with Bolt-Hole Clearances. *Composites Part B: Engineering*, **138**, 194-205. https://doi.org/10.1016/j.compositesb.2017.11.027

[34] Li, H., Zhang, K., Cheng, H., Suo, H., Cheng, Y. and Hu, J. (2019) Multi-Stage Mechanical Behavior and Failure Mechanism Analysis of CFRP/Al Single-Lap Bolted Joints with Different Seawater Ageing Conditions. *Composite Structures*, **208**, 634-645. https://doi.org/10.1016/j.compstruct.2018.10.044

[35] Riccio, A. and Marciano, L. (2005) Effects of Geometrical and Material Features on Damage Onset and Propagation in Single-Lap Bolted Composite Joints under Tensile Load: Part I—Experimental Studies. *Journal of Composite Materials*, **39**, 2071-2090. https://doi.org/10.1177/0021998305052026

[36] McCarthy, M.A., Lawlor, V.P. and Stanley, W.F. (2005) An Experimental Study of Bolt-Hole Clearance Effects in Single-Lap, Multibolt Composite Joints. *Journal of Composite Materials*, **39**, 799-825. https://doi.org/10.1177/0021998305048157

[37] Hu, J., Zhang, K., Cheng, H. and Qi, Z. (2020) Mechanism of Bolt Pretightening and Preload Relaxation in Composite Interference-Fit Joints under Thermal Effects. *Journal of Composite Materials*, **54**, 4929-4946. https://doi.org/10.1177/0021998320941218

[38] Yang, B., Yue, Z., Geng, X., Guan, X. and Wang, P. (2016) Experimental and Numerical Study on Bearing Failure of Countersunk Composite-Composite and Composite-steel Joints. *Journal of Composite Materials*, **51**, 3211-3224. https://doi.org/10.1177/0021998316684936

[39] McCarthy, M.A., Lawlor, V.P., Stanley, W.F. and McCarthy, C.T. (2002) Bolt-Hole Clearance Effects and Strength Criteria in Single-Bolt, Single-Lap, Composite Bolted Joints. *Composites Science and Technology*, **62**, 1415-1431. https://doi.org/10.1016/s0266-3538(02)00088-x

[40] Choi, J., Hasheminia, S.M., Chun, H., Park, J. and Chang, H.S. (2018) Failure Load Prediction of Composite Bolted Joint with Clamping Force. *Composite Structures*, **189**, 247-255. https://doi.org/10.1016/j.compstruct.2018.01.037

[41] Arman, Y. (2012) Effect of Washer Type on Bearing Strength of Bolted-Joint Laminated Composites. *Advanced Composites Letters*, **21**.

[42] Oh, J.H., Kim, Y.G. and Lee, D.G. (1997) Optimum Bolted Joints for Hybrid Composite Materials. *Composite Structures*, **38**, 329-341. https://doi.org/10.1016/s0263-8223(98)80014-7

[43] Chang, F., Scott, R.A. and Springer, G.S. (1982) Strength of Mechanically Fastened

Composite Joints. *Journal of Composite Materials*, **16**, 470-494. https://doi.org/10.1177/002199838201600603

[44] Gamdani, F., Boukhili, R. and Vadean, A. (2015) Tensile Strength of Open-Hole, Pin-Loaded and Multi-Bolted Single-Lap Joints in Woven Composite Plates. *Materials & Design*, **88**, 702-712. https://doi.org/10.1016/j.matdes.2015.09.008

[45] Liu, L.Q. (2022) A Study of the Damage Tolerance of Composite-Metal Hybrid Joints Reinforced by Multiple and Penetrative Thin Pins. *Composites and Advanced Materials*, **31**, 1-13.

[46] Walker, S.P. (2002) Thermal Effects on the Pin-Bearing Behavior of IM7/PETI5 Composite Joints. *Journal of Composite Materials*, **36**, 2623-2651. https://doi.org/10.1177/002199802761675557

[47] Gupta, A. and Singh, M. (2024) Comparative Study of Failure Analysis in Glass Fiber Reinforced Laminated Pin Joints under Cyclic and Static Loading Conditions. *Journal of Composite Materials*, **58**, 661-675. https://doi.org/10.1177/00219983241230386

[48] Choi, J. and Chun, Y. (2003) Failure Load Prediction of Mechanically Fastened Composite Joints. *Journal of Composite Materials*, **37**, 2163-2177. https://doi.org/10.1177/002199803038108

[49] Abazadeh, B. and Maleki, H. (2021) Effect of Bolt Tightening on the Fatigue Behavior of GLARE Double Shear Lap Joints. *Journal of Composite Materials*, **55**, 2911-2920. https://doi.org/10.1177/00219983211003315

[50] Van Rooijen, R.G.J., Sinke, J., De Vries, T.J. and Van Der Zwaag, S. (2006) The Bearing Strength of Fiber Metal Laminates. *Journal of Composite Materials*, **40**, 5-19. https://doi.org/10.1177/0021998305053509

[51] Ferret, B., Anduze, M. and Nardari, C. (1998) Metal Inserts in Structural Composite Materials Manufactured by RTM. *Composites Part A*: *Applied Science and Manufacturing*, **29**, 693-700. https://doi.org/10.1016/s1359-835x(97)00107-3

[52] Camanho, P.P., Tavares, C.M.L., de Oliveira, R., Marques, A.T. and Ferreira, A.J.M. (2005) Increasing the Efficiency of Composite Single-Shear Lap Joints Using Bonded Inserts. *Composites Part B*: *Engineering*, **36**, 372-383. https://doi.org/10.1016/j.compositesb.2005.01.007

[53] Muc, A. and Ulatowska, A. (2012) Local Fibre Reinforcement of Holes in Composite Multilayered Plates. *Composite Structures*, **94**, 1413-1419. https://doi.org/10.1016/j.compstruct.2011.11.017

[54] Mara, V., Haghani, R. and Al-Emrani, M. (2016) Improving the Performance of Bolted Joints in Composite Structures Using Metal Inserts. *Journal of Composite Materials*, **50**, 3001-3018. https://doi.org/10.1177/0021998315615204

[55] Zhu, Y., Qin, Y., Qi, S., Xu, H., Liu, D. and Yan, C. (2018) Variable Angle Tow Reinforcement Design for Locally Reinforcing an Open-Hole Composite Plate. *Composite Structures*, **202**, 162-169. https://doi.org/10.1016/j.compstruct.2018.01.021

[56] Kolks, G. and Tserpes, K.I. (2014) Efficient Progressive Damage Modeling of Hybrid Composite/Titanium Bolted Joints. *Composites Part A*: *Applied Science and Manufacturing*, **56**, 51-63. https://doi.org/10.1016/j.compositesa.2013.09.011

[57] Camanho, P.P., Fink, A., Obst, A. and Pimenta, S. (2009) Hybrid Titanium-CFRP Laminates for High-Performance Bolted Joints. *Composites Part A*: *Applied Science and Manufacturing*, **40**, 1826-1837. https://doi.org/10.1016/j.compositesa.2009.02.010

[58] Petersen, E., Koord, J., Völkerink, O., Stefaniak, D. and Hühne, C. (2019) Experimental and Numerical Investigation of the Transition Zone of Locally Steel-Rein-

forced Joining Areas under Combined Tension-Bending Loading. *Journal of Composite Materials*, **54**, 2339-2352. https://doi.org/10.1177/0021998319893729

[59] Fink, A., Camanho, P.P., Andrés, J.M., Pfeiffer, E. and Obst, A. (2010) Hybrid CFRP/Titanium Bolted Joints: Performance Assessment and Application to a Spacecraft Payload Adaptor. *Composites Science and Technology*, **70**, 305-317. https://doi.org/10.1016/j.compscitech.2009.11.002

[60] Ren, M., Chang, X., Xu, H.Y. and Li, T. (2017) Trans-Scale Analysis of Composite Overwrapped Pressure Vessel at Cryogenic Temperature. *Composite Structures*, **160**, 1339-1347. https://doi.org/10.1016/j.compstruct.2016.10.126

[61] Saha, S., Sullivan, R.W. and Baker, M.L. (2023) Gas Permeability Mitigation of Cryogenically Cycled Stitched Composites Using Thin Plies. *Composite Structures*, **304**, Article ID: 116352. https://doi.org/10.1016/j.compstruct.2022.116352

[62] Fukui, H., Yoshimura, A. and Matsuzaki, R. (2016) Structural Optimization for CFRP Cryogenic Tank Based on Energy Release Rate. *Composite Structures*, **152**, 883-890. https://doi.org/10.1016/j.compstruct.2016.06.004

[63] Liu, N., Ma, B., Liu, F., Huang, W., Xu, B., Qu, L., *et al*. (2021) Progress in Research on Composite Cryogenic Propellant Tank for Large Aerospace Vehicles. *Composites Part A*: *Applied Science and Manufacturing*, **143**, Article ID: 106297. https://doi.org/10.1016/j.compositesa.2021.106297

[64] Bang, C.S., Kim, J.G. and Lee, D.G. (2013) Performance Improvement by Glass Fiber of Adhesively Bonded Metal Joints at the Cryogenic Temperature. *Composite Structures*, **96**, 321-331. https://doi.org/10.1016/j.compstruct.2012.08.050

[65] Nam, S., Yu, Y.H., Choi, I., Bang, C.S. and Lee, D.G. (2014) Fracture Toughness Improvement of Polyurethane Adhesive Joints with Chopped Glass Fibers at Cryogenic Temperatures. *Composite Structures*, **107**, 522-527. https://doi.org/10.1016/j.compstruct.2013.08.015

[66] Kim, J.G., Hwang, Y.J., Yoon, S.H. and Lee, D.G. (2014) Improvement of the Fracture Toughness of Adhesively Bonded Stainless Steel Joints with Aramid Fibers at Cryogenic Temperatures. *Composite Structures*, **107**, 522-527.

[67] Reed, R.P. and Golda, M. (1994) Cryogenic Properties of Unidirectional Composites. *Cryogenics*, **34**, 909-928. https://doi.org/10.1016/0011-2275(94)90077-9

[68] Hohe, J., Neubrand, A., Fliegener, S., Beckmann, C., Schober, M., Weiss, K., *et al*. (2021) Performance of Fiber Reinforced Materials under Cryogenic Conditions—A Review. *Composites Part A*: *Applied Science and Manufacturing*, **141**, Article ID: 106226. https://doi.org/10.1016/j.compositesa.2020.106226

[69] Sápi, Z. and Butler, R. (2020) Properties of Cryogenic and Low Temperature Composite Materials: A Review. *Cryogenics*, **111**, Article ID: 103190. https://doi.org/10.1016/j.cryogenics.2020.103190

[70] Yan, M., Liu, Y., Jiang, W., Qin, W., Yan, Y., Wan, L., *et al*. (2022) Mechanism of Matrix Influencing the Cryogenic Mechanical Property of Carbon Fibre Reinforced Epoxy Resin Composite. *Composites Communications*, **33**, Article ID: 101220. https://doi.org/10.1016/j.coco.2022.101220

[71] Kim, M., Kang, S., Kim, C. and Kong, C. (2007) Tensile Response of Graphite/Epoxy Composites at Low Temperatures. *Composite Structures*, **79**, 84-89. https://doi.org/10.1016/j.compstruct.2005.11.031

[72] Huang, W.J., Li, Y.T., Zhang, Y.M., Xiao, Z.M. and Li, W.G. (2025) Experimental and Numerical Investigations of Interlaminar Shear Behaviors of CFRP Composites at Cryogenic and High Temperatures. *Composite Structures*, **352**, Article ID: 118681.

https://doi.org/10.1016/j.compstruct.2024.118681

[73] Soykok, I.F., Sayman, O. and Ozen, M. (2012) Low Temperature and Tightening Torque Effects on the Failure Response of Bolted Glass Fiber/Epoxy Composite Joints. *Journal of Composite Materials*, **47**, 3257-3268. https://doi.org/10.1177/0021998312463828

[74] Khashaba, U.A. (2018) Static and Fatigue Analysis of Bolted/Bonded Joints Modified with CNTs in CFRP Composites under Hot, Cold and Room Temperatures. *Composite Structures*, **194**, 279-291. https://doi.org/10.1016/j.compstruct.2018.04.008

[75] Koord, J. and Hühne, C. (2024) Bolt-Bearing Behavior of Hybrid CFRP-Steel Laminates at Low Temperature. *Journal of Composite Materials*, **58**, 2443-2455. https://doi.org/10.1177/00219983241262955

[76] Touloukian, Y.S. and Ho, C.Y. (1977) Physical Properties of Selected Aerospace Materials Part II, Thermophysical Properties of Seven Materials. AD A1, 29295, CIN-DAS, Purdue University.

[77] Hust, J.G. (1984) Thermal Conductivity of Glass 1 Fiber/Epoxy Composite Support Bands for Cryogenic Dewars, Phase II. NBSIR 84-3003, National Bureau of Standards, U.S. Department of Commerce.

[78] Larsen, T.Ø., Andersen, T.L., Thorning, B., Horsewell, A. and Vigild, M.E. (2007) Comparison of Friction and Wear for an Epoxy Resin Reinforced by a Glass or a Carbon/Aramid Hybrid Weave. *Wear*, **262**, 1013-1020. https://doi.org/10.1016/j.wear.2006.10.004

[79] Schmitt, C., Kremeur, A., Lipinski, P. and Capelle, J. (2024) Numerical Optimization by Finite Element Method of Stainless Steel/Glass-Epoxy Composite Bolted Joint under Tension and Compression. *Engineering*, **16**, 102-122. https://doi.org/10.4236/eng.2024.164009

[80] Mínguez, J.M. and Vogwell, J. (2006) Effect of Torque Tightening on the Fatigue Strength of Bolted Joints. *Engineering Failure Analysis*, **13**, 1410-1421. https://doi.org/10.1016/j.engfailanal.2005.10.012

[81] Liu, F., Lu, X., Zhao, L., Zhang, J., Xu, J. and Hu, N. (2018) Investigation of Bolt Load Redistribution and Its Effect on Failure Prediction in Double-Lap, Multi-Bolt Composite Joints. *Composite Structures*, **202**, 397-405. https://doi.org/10.1016/j.compstruct.2018.02.043

[82] Jiang, Z., Wan, S., Fang, Z. and Song, A. (2021) Static and Fatigue Behaviours of a Bolted GFRP/Steel Double Lap Joint. *Thin-Walled Structures*, **158**, Article ID: 107170. https://doi.org/10.1016/j.tws.2020.107170

[83] Gao, Y., Zhang, D., Li, F., Zhao, Q., Zhao, Z. and Chen, Y. (2021) Bearing Strength and Failure Behaviour of Composite Pre-Tightened Multi-Tooth Joint. *Composite Structures*, **272**, Article ID: 114208. https://doi.org/10.1016/j.compstruct.2021.114208

[84] Khashaba, U.A., Sallam, H.E.M., Al-Shorbagy, A.E. and Seif, M.A. (2006) Effect of Washer Size and Tightening Torque on the Performance of Bolted Joints in Composite Structures. *Composite Structures*, **73**, 310-317. https://doi.org/10.1016/j.compstruct.2005.02.004

[85] Zhu, Y. and Xiong, J. (2022) Temperature Effect on Mechanical Performances and Failure Mechanisms of Single-Lap Countersunk-Screwed CFRPI-Metal Joint. *Composite Structures*, **289**, Article ID: 115459. https://doi.org/10.1016/j.compstruct.2022.115459

[86] He, B.L. (2020) Experimental and Semi-Analytical Investigation of X850 ± IM190

CFRP Bolted Joints. *Composites and Advanced Materials*, **29**, 1-12. https://doi.org/10.1177/0963693519895009

[87] Kolesnikov, B., Herbeck, L. and Fink, A. (2008) CFRP/Titanium Hybrid Material for Improving Composite Bolted Joints. *Composite Structures*, **83**, 368-380. https://doi.org/10.1016/j.compstruct.2007.05.010

Abbreviation List

CT: Cryogenic Temperature
LT: Low Temperature
RT: Room Temperature
Nomenclature
d_{1s} : external diameter of the first cylindrical insert
d_{2s} : external diameter of the second cylindrical insert
E_{st} : Young's modulus of stainless steel
E_x, E_y, E_z : Young's moduli of woven glass-epoxy composite material
F^e : critical force
F^e_{CT} : Critical force and stress at CT
F^e_{RT} : Critical force and stress at RT
F^f : failure force
F^u : ultimate force
F^u_{RT} : Ultimate force at RT
F^u_{CT} : Ultimate force at CT
G_{xy}, G_{yz}, G_{xz} : Coulomb's moduli of woven glass-epoxy composite material
$k^{\mathrm{I}}_{\mathrm{CT}}$: slope of the curves in linear stage I at CT
$k^{\mathrm{I}}_{\mathrm{RT}}$: slope of the curves in linear stage I at RT
$k^{\mathrm{III}}_{\mathrm{CT}}$: Stiffness of the bolted joint at CT
$k^{\mathrm{III}}_{\mathrm{RT}}$: Stiffness of the bolted joint at RT
$\overline{k}^{\mathrm{III}}_{\mathrm{CT}}$: mean value of stiffness of the bolted joint at CT
$\overline{k}^{\mathrm{III}}_{\mathrm{RT}}$: mean value of stiffness of the bolted joint at RT
K_t : stress concentration factor
$K_t^{(i)}$: stress concentration factor for configuration "*i*"
l_c : length of hybrid composite material plate
l_s : length of stainless-steel external plates
t_c : thickness of hybrid composite material plate
t_l : thickness of each layer of hybrid composite material
t_s : thickness of stainless-steel external plates
u^e : ultimate load displacement
w_c : width of hybrid composite material plate
w_s : width of stainless-steel external plates
$\overline{\overline{\alpha}}$: tensor of expansion coefficients
$\overline{\overline{\varepsilon}}^{th}$: tensor of thermal strain
λ : thermal conductivity
ν_{st} : Poisson's ratio of stainless steel
$\nu_{xy}, \nu_{yz}, \nu_{zx}$: Poisson's ratios of woven glass-epoxy composite material
σ_{eb} : yield strength of stainless-steel bolt
σ_{ub} : ultimate strength of stainless-steel bolt
$\sigma^{\mathrm{nom}}_{xx}$: nominal tensile stress
ΔT : increment of temperature